Realizing the 'hindered charge ordered phase' in nanoscale charge ordered manganites: magnetization, magneto-transport and EPR investigations

2009 J. Phys.: Condens. Matter 21 196005

(http://iopscience.iop.org/0953-8984/21/19/196005)

J. Phys.: Condens. Matter **21** (2009) 196005 (13pp) doi:10.1088/0953-8984/21/19/196005

Realizing the 'hindered charge ordered phase' in nanoscale charge ordered manganites: magnetization, magneto-transport and EPR investigations

S S Rao and S V Bhat

Department of Physics, Indian Institute of Science, Bangalore, India

E-mail: ssrao@physics.iisc.ernet.in and svbhat@physics.iisc.ernet.in

Received 4 October 2008, in final form 14 January 2009
Published 22 April 2009
Online at stacks.iop.org/JPhysCM/21/196005

Abstract

We report three prominent observations made on the nanoscale charge ordered (CO) manganites $RE_{1-x}AE_xMnO_3$ (RE = Nd, Pr; AE = Ca; $x = 0.5$) probed by temperature dependent magnetization and magneto-transport, coupled with electron magnetic/paramagnetic resonance spectroscopy (EMR/EPR). First, evidence is presented to show that the predominant ground state magnetic phase in nanoscale CO manganites is ferromagnetic and it coexists with a residual anti-ferromagnetic phase. Secondly, the shallow minimum in the temperature dependence of the EPR linewidth shows the presence of a charge ordered phase in nanoscale manganites which was shown to be absent from the DC static magnetization and transport measurements. Thirdly, the EPR linewidth, reflective of spin dynamics, increases significantly with a decrease of particle size in CO manganites. We discuss the interesting observations made on various samples of different particle sizes and give possible explanations. We have shown that EMR spectroscopy is a highly useful technique to probe the 'hindered charge ordered phase' in nanoscale CO manganites, which is not possible by static DC magnetization and transport measurements.

(Some figures in this article are in colour only in the electronic version)

1. Introduction

Manganites with the general formula $RE_{1-x}AE_xMnO_3$ (RE, rare earth ion like La, Pr, Nd etc and AE, alkaline earth ion like Ca, Sr, Ba etc), a class of strongly correlated systems, have drawn great interest owing to their intriguing science and possible technological applications [1–3]. Colossal magneto resistance (CMR) and charge ordering (CO), to name a few are well studied aspects of this class of materials in the form of single crystals, thin films and bulk polycrystalline compounds. However, recently several research groups have attempted to investigate the properties of CMR manganites in the form of nanoparticles, nanowires, nanotubes and nanocubes using various experimental probes [4–7]. There were no studies on the properties of nanoscale charge ordering manganites until we discovered and reported some novel findings recently [8, 9]. We have shown that the charge ordered phase is either weakened/suppressed, there is a switch over from the anti-ferromagnetic phase to the ferromagnetic phase, a size induced insulator to metal transition and 99.9% CMR (at 11 T) in nanoscale $Pr_{0.5}Ca_{0.5}MnO_3$ (PCMO) and $Nd_{0.5}Ca_{0.5}MnO_3$ (NCMO) [8, 9]. In particular, these results are very significant as one needs to use several external stimuli to *melt* the CO phase and in turn transform the anti-ferromagnetic (AFM) phase to the ferromagnetic (FM) phase in concurrence with the insulator–metal transition [10, 11]. Subsequently, several authors [12–17] have reported that the ground state properties of various charge ordered manganites having a range of melting strengths are highly modified with a reduction of particle size down to the nanoscale, confirming and supporting our earlier reported results [8, 9]. The phase diagram between the charge ordering temperature and the particle size has been constructed and was reported by Zhang *et al* [16], although the exact mechanism for the

modification of the CO phase with the particle size is still intensely debated [8, 9, 12–17]. Very recently [17], Dong *et al* have performed theoretical calculations using Monte Carlo techniques coupled with a two orbital double exchange model on half doped nanoscale charge exchange (CE) type CO manganites. It was shown that the CE charge ordered phase is suppressed and a weak ferromagnetic signal emerges. However, the following questions are still unanswered and need to be addressed. (a) What is the predominant ground state magnetic phase? (b) What are the coexisting magnetic phases? (c) To what extent is the CO phase destabilized? (d) Does the CO phase disappear completely in nanoscale CO manganites? To answer the above questions, extensive studies have been made through magnetization, magneto-transport and EPR spectroscopic measurements performed on NCMO and PCMO nanomanganites. In our earlier publication [18], it was reported that EPR spectroscopy gives evidence for the occurrence of charge ordering fluctuations in $Pr_{0.57}Ca_{0.41}Ba_{0.02}MnO_3$ nanoscale manganites through the temperature dependence of the EPR linewidth, although the static DC magnetization measurements had shown the complete absence of a CO phase. In the current paper, we report the results obtained from extensive studies employing three distinct experimental probes, namely, static DC magnetization, magneto-transport and electron magnetic resonance measurements, in order to investigate the occurrence/absence of a CO phase. From these results, we show that EPR spectroscopy is proved to be an excellent technique (by taking advantage of its sensitivity and relatively fast timescales) to investigate the *presence of a CO phase in nanomanganites* as the static DC magnetization (M–T), magneto-transport (R–T) and x-ray diffraction measurements had shown the complete absence of a CO phase, as reported earlier [8, 9, 12–17] and in this current article as well. We found that *EPR linewidth increases significantly* with a decrease of particle size down to the nanoscale in NCMO and PCMO nanoparticles in the charge disordered paramagnetic (PM) phase.

The EPR technique has long been used to study the properties of strongly correlated systems, such as manganites, as a local dynamical condensed matter probe. EPR gives significant information related to magnetic phase transitions, magnetic anisotropy, magnetic heterogeneity and magnetic phase separation on single crystals, thin films and bulk polycrystalline materials, as has been widely reported [19–21]. In particular, it was well established and reported that EPR gives benchmark signatures of a charge ordered phase in manganites through the strong temperature dependences of the EPR spectral parameters, namely, linewidth, g-value and integrated intensity [22, 23]. Joshi *et al* have shown that the temperature dependence of EMR linewidth goes through a minimum at the charge ordering temperature (T_{CO}) in bulk single crystal and polycrystalline NCMO [22]. In this paper, we show the effect of particle size on the EPR linewidth in two classic and prototype charge ordered manganites NCMO and PCMO, although we have obtained similar results in several other charge ordered manganites [24, 25]. The bulk NCMO and PCMO show a charge ordered phase at $T_{CO} = 250$ K, 245 K and an anti-ferromagnetic phase at $T_N = 160$ K, 175 K respectively while cooling from room temperature; both systems exhibit insulating behaviour below 300 K [26, 27].

2. Experimental methods

The nanoparticles of NCMO and PCMO were prepared by the polymer assisted sol–gel method [9]. Several samples of NCMO with increasing average particle sizes 10, 20, 40 nm (NCMO 10, NCMO 20, NCMO 40) and PCMO with increasing average particle sizes of 10, 20, 40 nm (PCMO 10, PCMO 20, PCMO 40) were obtained by following systematic calcination steps. The corresponding bulk compounds (NCMO BULK, PCMO BULK) were synthesized by a standard solid state reaction route. A variety of techniques such as x-ray diffraction (XRD), transmission electron microscopy (TEM) and magnetization measurements (using PPMS-VSM, QUANTUM DESIGN) were used to characterize the materials fully and to study the size dependence of the magnetic properties on tightly packed samples. From the x-ray diffraction studies, we found that all the materials (NCM 10, NCMO 20, NCMO 40) are single phase (perovskite) in nature without any secondary phase. TEM studies have shown that the particles are single crystalline, agglomerated. The average particle sizes are 10 nm (±3 nm), 20 nm (±3 nm) and 40 nm (±2 nm)for NCMO 10, NCMO 20 and NCMO 40 respectively. A few of these characterization details were published earlier [9]. The EMR studies were performed using a Bruker EMX X-band ESR spectrometer operating at 9.43 GHz by sweeping the magnetic field from 0 to 14 900 G from room temperature down to a temperature of 4 K on all the samples. The samples were diluted by paraffin wax to minimize the inter particle interactions. DPPH (2,2-diphenyl-1-picrylhydrazyl) was used as a field marker.

3. Results and discussion

The remainder of this paper is organized as follows, divided into three broad sections. In section 3.1, we present and discuss various interesting magnetization results obtained on several samples by varying the temperature and magnetic field. This is followed by section 3.2, devoted to describing the temperature and field dependent magneto-transport results. In section 3.3, we discuss the important results obtained from the temperature dependent electron paramagnetic resonance (EPR) spectroscopic measurements recorded on particles of various sizes and their comparison with those of the bulk compound.

3.1. Magnetization measurements

Figure 1(a) shows the temperature dependent magnetization of NCMO 10 measured under varying conditions from 2 K → 300 K. The curve shown with the symbol ■ plots magnetization versus temperature when the measurements were taken during the heating run, with the measurement field at 1 T, after the sample was cooled down to the lowest temperature in zero field (ZFC, 1 T). No indication of a CO peak at around 250 K is seen, and a sudden rise in magnetization at around 150 K indicates the onset of

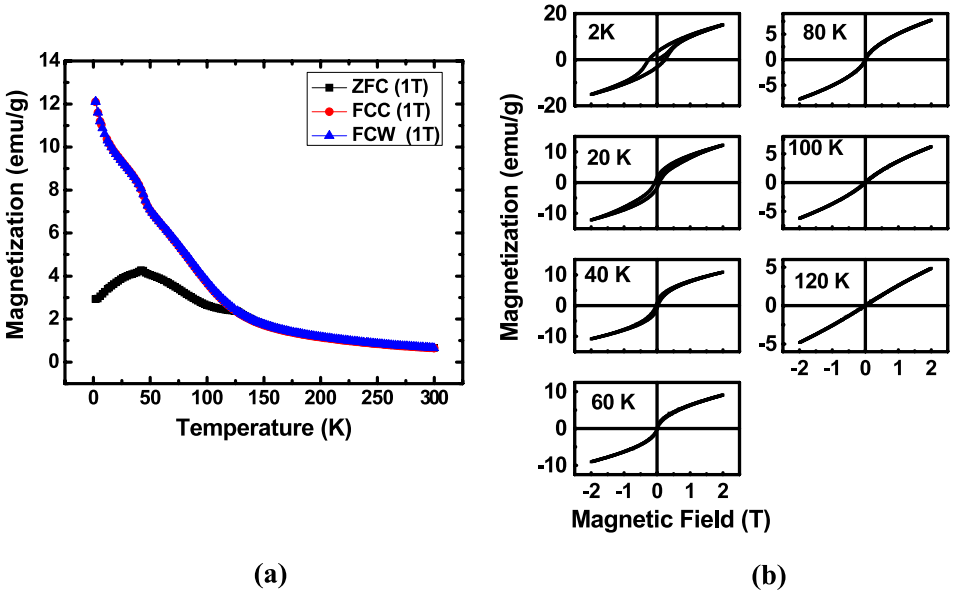

Figure 1. (a) Variation of magnetization with the temperature of NCMO 10 under zero field cooled (ZFC at 1 T), field cooled cooling (FCC, at 1 T) and field cooled warming (FCW, at 1 T) conditions. (b) Isothermal M–H loops of NCMO 10 measured at different temperatures at (2, 20, 40, 60, 80, 100 and 120 K) by sweeping the magnetic field from $0 \rightarrow 2\ \mathrm{T} \rightarrow 0 \rightarrow -2\ \mathrm{T} \rightarrow 0 \rightarrow 2\ \mathrm{T}$.

ferromagnetic phase. The peak at 50 K indicates the 'blocking temperature (T_b)' [28]. Field cooled cooling (FCC) and field cooled warming (FCW) measurements have been performed on NCMO 10 at 1 T and the results are shown in the same figure. In this figure, the curves with the symbols ● (red) and ▲ (blue) depict the FCC and FCW at 1 T respectively. It is clear that no CO peak is observed in either of the curves and a sudden rise in magnetization at around 150 K is seen. Non-hysteretic magnetization behaviour is observed between FCC and FCW at 1 T, indicating the occurrence of a first order phase transition (FOPT). Therefore it is concluded from the magnetization measurements that the CO phase is suppressed in NCMO 10. Figure 1(b) shows the isothermal magnetization behaviour of NCMO 10 at different temperatures (2, 20, 40, 60, 80, 100 and 120 K) with the magnetic field sweeping from $0 \rightarrow 2\ \mathrm{T} \rightarrow 0 \rightarrow -2\ \mathrm{T} \rightarrow 0 \rightarrow 2\ \mathrm{T}$. As is clearly seen from this graph, the M–H hysteresis loop area keeps on increasing with a decrease in temperature from 120 to 2 K, indicating the presence of a ferromagnetic phase below 120 K. The inverse of magnetization against the temperature is plotted for NCMO 10, NCMO 20 and NCMO 40 from 150 to 300 K and the experimental data is fitted to the Curie–Weiss law in the paramagnetic phase (figure 2). It is observed that there is a small deviation from the fits in NCMO 10 around 225 K and the deviation increases with an increase of particle size, indicating an increasing fraction of charge ordered phase with the particle size.

Extensive magnetization measurements were performed by following the novel protocol in order to study the nature of the ground state magnetic phase and to investigate the coexisting magnetic phases in NCMO 10 and NCMO 40. Isothermal magnetization measurements were performed on NCMO 10 and NCMO 40 at 5 K by sweeping the magnetic field from $0 \rightarrow 14\ \mathrm{T}$ (limit of our magnetic field) $\rightarrow 0 \rightarrow$

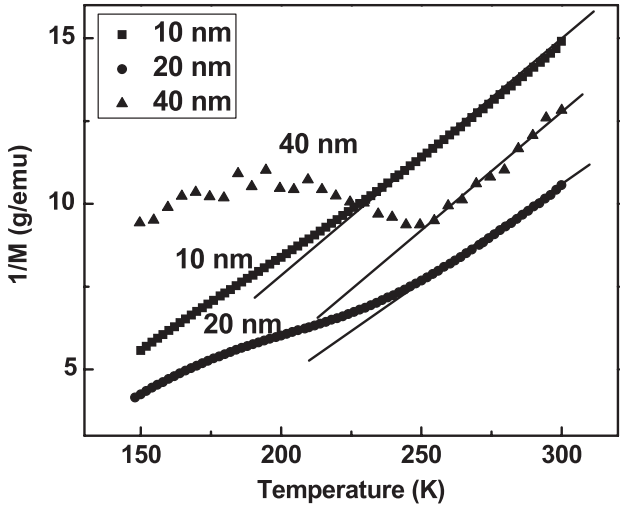

Figure 2. Curie–Weiss fit to the experimental data between 150 and 300 K of NCMO having different particle sizes 10, 20 and 40 nm.

$14\ \mathrm{T} \rightarrow 0$ and the results are shown in figures 3(a) and (b) respectively. Importantly, it is observed that the virgin M–H curves (I) lie outside the subsequent field cycling curves (II, III) in both NCMO 10 and NCMO 40. As shown in figure 3(b) for NCMO 40, in the virgin cycle (I), the increase of M with H resembles typical AFM behaviour until about 6 T, a sharp rise in the magnetization (M) is then observed until about 11 T, indicating a broad field induced transition, followed by a slower linear increase up to our limit of 14 T. The field decreasing cycle (II) shows hysteresis while approaching zero field. However, in the next field increasing cycle (III), the magnetization does not follow the virgin cycle (I) but rather follows the field decreasing cycle (I) with minimal hysteresis. A larger M–H hysteresis is observed in NCMO 40 when

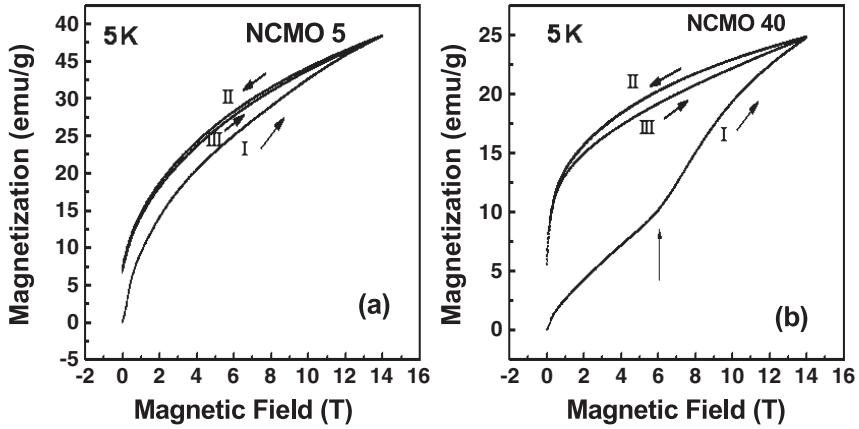

Figure 3. Isothermal M–H (virgin curve I, field decreasing II, next field increasing III curves) results obtained at 5 K on NCMO 10 (a) and NCMO 40 (b), respectively, with the magnetic field cycled between forward and reverse directions as shown in the figure with the pointed arrow from 0 → 14 T → 0 → 14 T. The black vertical arrow (figure(b)) shows the field induced first order phase transition (FOPT) from the residual anti-ferromagnetic phase to the ferromagnetic phase.

compared to NCMO 10, as observed from figure 3(a). There is a sudden rise in the magnetization of NCMO 40 at around 6 T, indicating a first order magnetic phase transition (FOPT) from the residual anti-ferromagnetic charge ordered phase to a ferromagnetic phase, although the classical saturation magnetization (3.5 μ_β/f.u.) was not attained even at 14 T. Such a rise in magnetization is not observed in NCMO 10 in the magnetic field cycles as it is mostly ferromagnetic at that temperature (5 K). NCMO 10 does not attain the full theoretical saturation magnetization value 3.5 μ_β/f.u., even at 14 T, at the temperature 5 K. Hence, it is inferred that a residual charge ordered anti-ferromagnetic phase may still be present in NCMO 10 even at a magnetic field of 14 T and at 5 K. This particular result is very significant, as it shows that the field required to induce the first order phase transition has been reduced drastically down to 6 T against about 20 T, as in the case of pristine bulk NCMO [1].

One way to explain this observation (the M_S being less for nanoparticles in comparison with the expected classical value) is by invoking the presence of a magnetic dead layer/shell, where the surface spins are practically paramagnetic/less ferromagnetic and the spins are localized on the particle shell. The effect of this non-magnetic surface layer is more prominent at the lowest particle size as observed in the CMR nanomanganites [4]. This large decrease in the saturation magnetization can also be related to the presence of non-collinear spins, magnetic dead layer (MDL). In addition, part of the magnetization reduction can be caused by the fact that the presence of a residual charge ordered phase inhibits the complete transformation of the material towards the ferromagnetic phase [29]. However, this explanation seems to be in contradiction to the model given by Dong *et al* for CO nanomanganites [30]. According to this model, the ferromagnetic layer and the corresponding ferromagnetic volume increase with a decrease of particle size in the charge ordered nanomanganites. Hence, at present the definitive reason for the observation of a lower saturation magnetization than expected is not clear.

Now we address the possible reasons for the observation of the virgin curve lying outside the envelope. Figure 3(b) shows the magnetization curves taken at 5 K on NCMO 40. The magnetization shows a sharp rise at a magnetic field of 6 T; this is the field at which the M–H curve changes the curvature from convex to concave. A large hysteresis is observed between the virgin curve and the envelope curve. A sharp rise in the magnetization accompanied by hysteresis is traditionally taken as a first order magnetic phase transition. This hysteresis is different from that normally observed in hard ferromagnets (virgin curve lies inside the envelope curve). The hysteresis in the case of a ferromagnet, which is due to domain wall pinning and/or anisotropy has a maximum width at $H = 0$, while in the present case the width almost goes to zero as H (magnetic field) tends to zero. It is also argued that the surface/volume ratio plays an important role in the observation of this uncommon relation between the virgin curve and the envelope curve in granular magnetic materials [31, 32]. Manekar and co-authors have observed, from the isothermal M–H and R–H measurements on doped $CeFe_2$, that the virgin curve anomalously falls outside the envelope hysteresis curve at low temperature. They attributed this to a glass-like arresting of the kinetics of the FM–AFM transition as the temperature is lowered [33]. The fact that the virgin curve lies outside the envelope loop could also be indicative of some irreversible pinning and depinning effects [34]. This kind of anomaly is also observed in LPCMO nanotubes, these are called inhomogeneous ferromagnetic nanooxides [29], whereas in the case of homogeneous ferromagnetic nanooxides such as LCMO and LSMO nanotubes, the virgin curve lies inside the envelope curve. Figure 4 plots the temperature dependent magnetization measured on NCMO 40 under varying conditions. As shown in this figure, a broad hump around temperature 250 K, shows the presence of a CO phase in NCMO 40. Hysteretic behaviour is observed between FCC and FCW at 4 T from 35 K to 150 K, indicating the first order magnetic phase transition. The magnetization behaviour with temperature for the FA 2 T and FA 6 T curves differ from

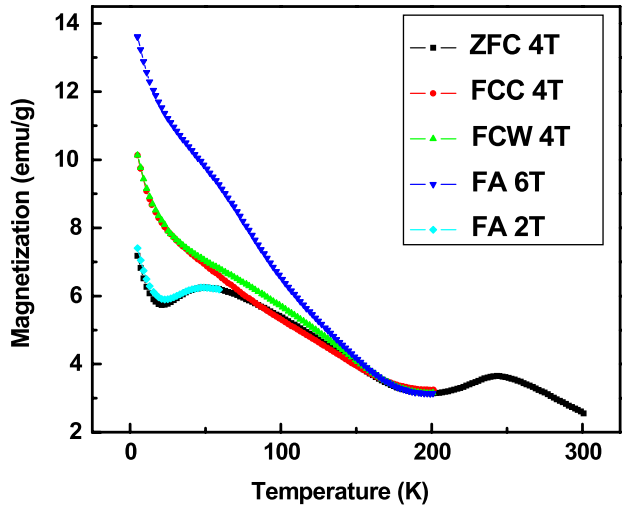

Figure 4. After cooling NCMO 40 in 2 and 6 T the field is isothermally changed to 4 T at 5 K and the magnetization is measured while warming (FA 2 T, FA 6 T). The variation of magnetization with temperature in zero field cooling, field cooled cooling and warming at 4 T is shown as ZFC 4 T, FCC 4 T and FCW 4 T.

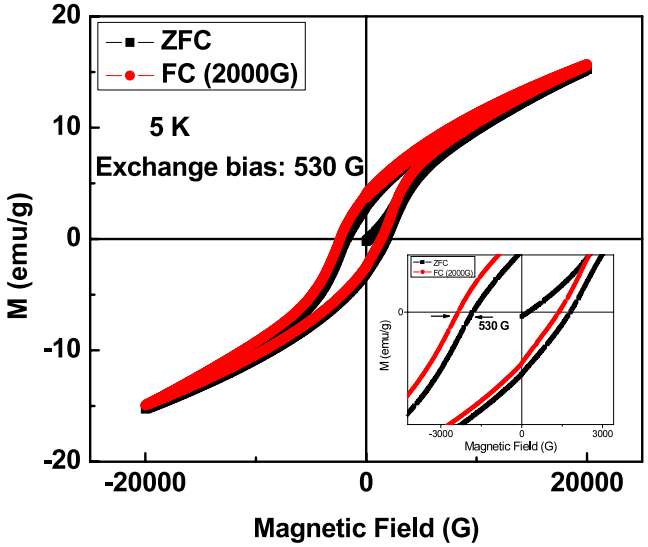

Figure 5. Isothermal M–H results obtained at 5 K on NCMO 10 for ZFC (in black) and FC (2000 G, in red) measurements; the measured exchange bias (E_b) is 530 G. The inset shows an enlarged view around zero magnetic field.

each other, and from that of the ZFC 4 T curve. Moreover, multiple values of magnetization at the same temperature and field indicate that there are different fractions of coexisting phases. Significantly, they evolve differently on warming, depending on whether the cooling field is higher or lower than the measuring field. Since there is a multiplicity of coexisting phases at the same temperature and field, it is an important issue to detect which one is the equilibrium phase and also the nature of the others. From figure 3(b), it is clear that once the field induced first order process converts the system to the FM phase it remains in the same state, implying that the original AFM phase is not the equilibrium phase at low temperature. This is consistent with the fact that the thermodynamic first ordered phase transition is triggered from the AF to the FM phase with a decrease in temperature. Nevertheless, cooling in a higher field results in a higher fraction of the FM phase at the lowest temperature in the same measurement field. This clearly indicates that there is some hindrance to the AF to FM phase transformation, which is alleviated by increasing the magnetic field. This hindrance brings about metastability in the remaining AF phase fraction at low-T, which is clearly demonstrated by all the M–T curves for which cooling fields are less than the measurement field. During warming, the metastable AF phase relaxes to the FM phase, concomitantly the magnetization increases with an increase in temperature. With a further increase in temperature, the usual course of reverse transformation to the AF phase takes place and magnetization decreases. On the contrary, the M–T curves for which cooling fields are more than the measurement field do not show these two opposing processes, the magnetization monotonically decreases with an increase in temperature. Similar behaviour is also observed in PCMO 20 and PCMO 40 (not shown). These interesting features corresponding to NCMO 40 can be associated with the competition between the residual charge ordered anti-ferromagnetic and ferromagnetic phases. Here, we would like to point out that this study clearly brings out the various generic features associated with a first order transition; namely, the appearance of hysteresis and the coexistence of different magnetic phases [35, 36].

To determine the presence of a residual anti-ferromagnetic charge ordered phase in NCMO 10, field cooled (FC) isothermal field dependent magnetization (FC MH) experiments at 5 K were performed in the presence of 0.2 T, and the results compared with those of zero field cooled (ZFC MH) measurements. The comparison is shown in figure 5. The curve in black shows ZFC MH and the curve in red shows FC MH. The inset of this figure shows an expanded view around zero magnetic field, where an exchange bias (or loop shift, E_b) of 530 G is observed at 5 K, giving clear evidence for the presence of a residual charge ordered anti-ferromagnetic phase coexisting with the predominant size induced ferromagnetic phase.

3.2. Magneto-transport measurements

Four probe resistivity measurements were conducted to study the electrical transport behaviour of these nanoscale materials. For the four probe resistivity measurements, pellets were prepared under a pressure of 150 psi and then sintered at 300 °C for 2 h, these parameters ensuring that the particle size did not increase and similar to the procedure followed by us previously [9]. Silver paste was used to make contacts to the electrodes. Magneto-transport measurements were performed on NCMO 10 and NCMO 20 by sweeping the temperature and magnetic fields. As shown in figure 6, NCMO BULK shows an insulating behaviour throughout the temperature range studied. In the same figure, the variation of ln R with temperature is plotted for NCMO 10 and NCMO 20 in the absence of a magnetic field. As can be seen, these two materials exhibit an insulator–metal transition at around 75 K;

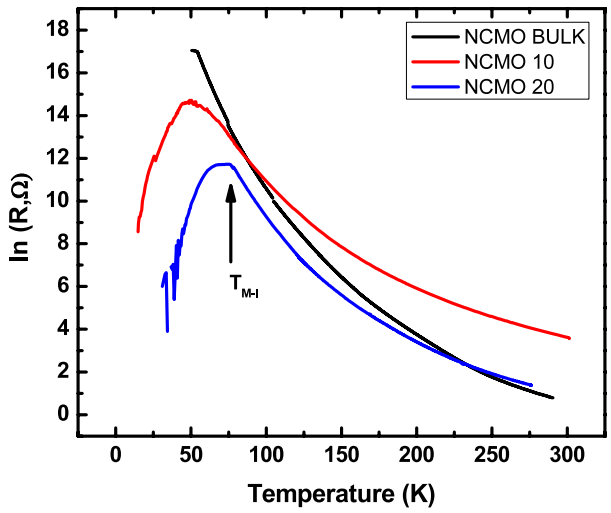

Figure 6. Variation of ln R (R = resistance) with temperature for NCMO 10, NCMO 20 and NCMO BULK in the absence of a magnetic field.

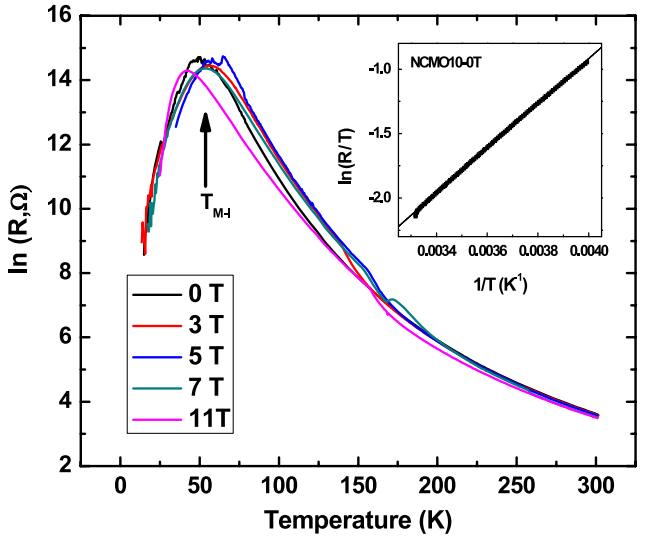

Figure 7. Variation of ln R (R = resistance) with temperature for NCMO 10 at different magnetic fields of 0, 3, 5, 7 and 11 T. The pointed arrows indicate the insulator–metal transition ($T_{M–I}$). The inset to this figure shows the adiabatic polaron activated fit [37] to the resistance behaviour in the paramagnetic region of NCMO 10 under zero magnetic field. The solid line is the fit to the experimental data shown as a continuous dotted line.

a size induced insulator–metal transition. The observation of a size induced insulator–metal transition, reported [9] by us in the same material, is in accordance with the Zener double exchange mechanism at around the same temperature as the ferromagnetic phase has also been observed. In figure 7, the variation of ln R with temperature for NCMO 10 at various magnetic fields 0, 3, 5, 7 and 11 T is shown. It can be seen that there is a shift in $T_{M\text{-}I}$ towards high temperatures up to 5 T, and then a shift towards low temperatures with a further increase of magnetic field from 7 to 11 T. NCMO 20 also exhibits a similar behaviour (not shown) with the application of magnetic fields. The transport behaviour in the charge disordered insulating paramagnetic phase is described well by the adiabatic activated polaron hopping model [37] for all the nanomaterials and at different magnetic fields, as shown in the inset of figure 7 for NCMO 10 in the absence of a magnetic field. From the fitted results, it can be observed that the activation energy increases, with the decrease of particle size, from 140 meV (for NCMO BULK) to 149 meV (for NCMO 10) and decreases with an increase of the applied magnetic field.

Isothermal R–H curves for NCMO 10 are plotted at 60, 80 and 120 K in figures 8(a)–(c). The arrows indicate the magnetic field cycles in the forward and reverse directions from $0 \rightarrow 11\ \text{T} \rightarrow 0$. This material exhibits quite interesting resistive non-closure hysteresis loops, showing the presence of strong magnetic memory effects. At 60 K (figure 8(a)), the resistance rises suddenly with the magnetic field (positive magneto resistance) and drops gradually with a further increase in the magnetic field (negative magneto resistance) in the forward direction. In the reverse cycle of the magnetic field, there is a gradual rise in the resistance with a decrease of magnetic field until about 5 T, where it suddenly increases peaking at 4 T before decreasing slowly with a further decrease in the magnetic field. The positive magneto resistance disappears with an increase in temperature from 60 to 120 K, as shown in figures 8(b) and (c). In figure 9, the isothermal MR (MR% $= (\frac{\rho_0 - \rho_H}{\rho_0}) \times 100$) variation of NCMO 20 with

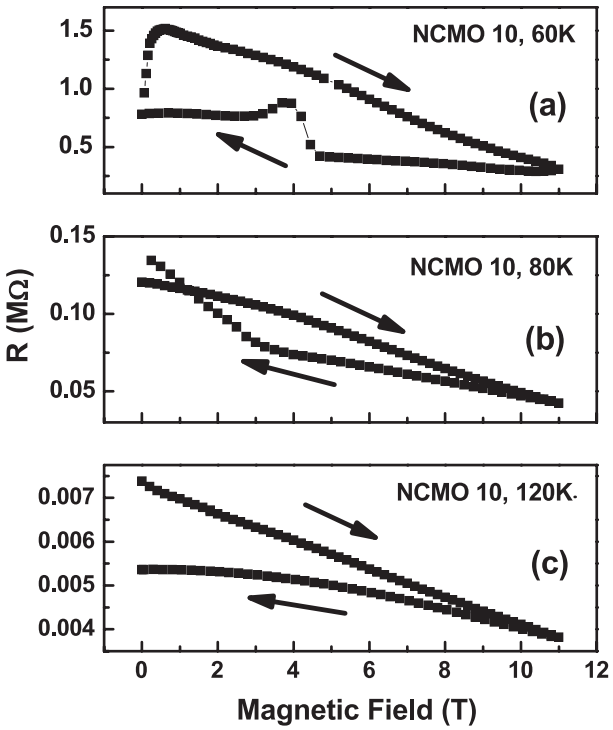

Figure 8. Isothermal variation of resistance R with magnetic field in the forward and reverse directions, as indicated by the arrows, for NCMO 10 measured at 60, 80 and 120 K.

magnetic field at 70, 100, 120 and 140 K is shown. Both positive and negative MR are observed in NCMO 20 at the lowest temperature studied, namely 70 K, (figure 9(d)). The positive MR disappears as the sample is warmed up from 70 to 140 K (figures 9(c)–(a)). From these figures, non-closure

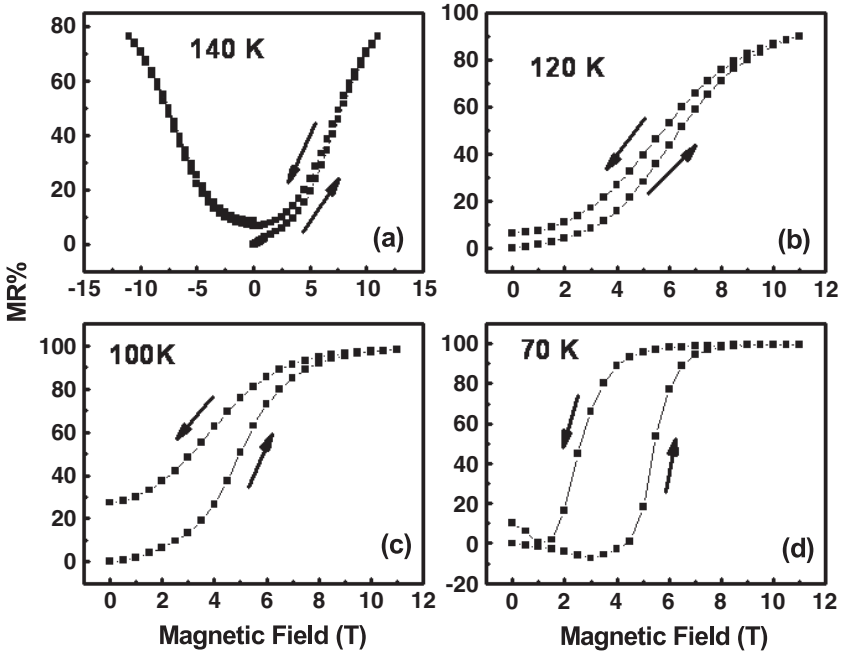

Figure 9. Isothermal MR (MR% $= (\frac{\rho_0 - \rho_H}{\rho_0}) \times 100$) variation of NCMO 20 with magnetic field swept in the forward and reverse directions ($0 \rightarrow 11$ T $\rightarrow 0 \rightarrow -11$ T $\rightarrow 0$), as indicated by the arrows, measured at different temperatures 70, 100, 120 and 140 K.

hysteretic R–H/MR–H loops are observed at 100, 120 and 140 K with decreasing loop area. These interesting features are the consequences of size induced ferromagnetism, metallicity and a destabilized CO phase; the CMR (99.7% at T_{M-I}, 11 T) is due to the extrinsic grain boundary effect. Similar non-closure and hysteretic R–H loops were observed in nanoring networks (NRN) of $La_{0.67}Ca_{0.33}MnO_3$, with dimensions 36 and 180 nm, by Zhu *et al* [38]. The observed low field magneto resistance (LFMR) and high field magneto resistance (HFMR) were explained by invoking the inelastic tunnelling model. The observed extrinsic magneto resistance in these nanoscale materials could make them good candidates for potential applications. The observed positive and negative magneto resistance from NCMO 10 and NCMO 20 at the lowest temperatures studied gives ample evidence to say that the ground state magnetic phase is a mixture of a residual charge ordered anti-ferromagnetic insulating phase and a predominant size induced ferromagnetic phase.

To briefly summarize the results from the above two sections, we have observed that the CO peak disappears gradually with a decrease of particle size from the bulk to nanoscale. In particular, no CO peak was observed in the temperature dependent magnetization measurements for NCMO 10 and NCMO 20 [9]. It was shown that the ferromagnetic phase is the dominant magnetic ground state with a residual anti-ferromagnetic phase. Four probe temperature dependent resistivity measurements have shown that the insulator to metal transition occurs at low temperatures in accordance with the Zener double exchange (DE) mechanism. Resistive hysteresis and CMR (99.7% at 11 T) are also observed in the magnetic field dependent transport measurements, which are the consequences of a destabilized charge ordered phase.

3.3. Electron paramagnetic resonance (EPR/EMR) measurements

In this section, we focus on the results obtained from the temperature dependent EMR/EPR measurements. As is evident from figure 10(a), the EMR signals are observed in NCMO 10 down to 10 K. The EMR signals below 120 K are highly asymmetric, distorted, and broadened, and shift towards low magnetic fields with a further decrease of temperature whilst gradually dropping in intensity. These are characteristic features of ferromagnetic signals [39, 8], thus confirming the presence of size induced ferromagnetism. Similar signals were also obtained from NCMO 20 and NCMO 40(not shown). All these materials (i.e. NCMO 10, NCMO 20, NCMO 40) show two well defined regimes in the thermal evolution of the EMR spectra. In the high temperature regime (120 K $< T <$ 300 K), the line shapes are symmetric, broad and Lorentzian in shape, as the effective anisotropy and the inter particle interactions are smoothed by thermal effects. The continuous lines in figure 10(a) show the experimental data and the dotted lines indicate the fitted curve using the following double Lorentzian line shape equation [21].

$$\left[\frac{\mathrm{d}P}{\mathrm{d}H}\right] = A\frac{\mathrm{d}}{\mathrm{d}H}\left(\frac{\Delta H}{4(H-H_0)^2+\Delta H^2} + \frac{\Delta H}{4(H+H_0)^2+\Delta H^2}\right), \quad (1)$$

where H_0 is the centre field, ΔH is the full width at half maximum, when divided by a factor of $\sqrt{3}$ it gives ΔH_{pp} (peak to peak linewidth), and A is a quantity proportional to the area under the curve. The two terms in the above equation describe the contributions from the clockwise and anti-clockwise circularly polarized components

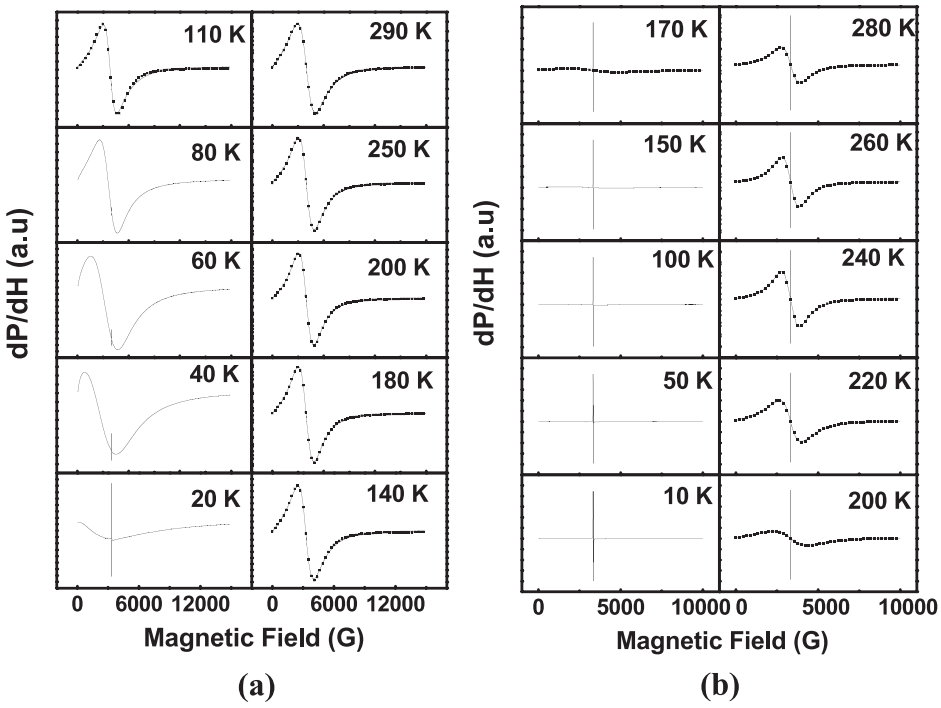

Figure 10. Thermal evolution of EPR/EMR signals originating from NCMO 10 (a) and NCMO BULK (b). The sharp line is due to DPPH.

of microwave radiation and is necessary to include these because of the large width of the signals, typical for charge ordered perovskite manganites [22, 23, 40, 41, 18]. This particular equation has been shown to give excellent fits for the broad EPR lines observed from the charge ordered manganites [22, 23, 40, 41, 18]. In the second regime (low temperatures), i.e., 20 K $< T <$ 120 K, the EMR signal is highly asymmetric, the resonance field and the linewidth do not follow the high temperature behaviour; the intensity does not follow the Curie–Weiss behaviour. The anisotropy enhancement can be associated with a larger surface anisotropy acting on the external surface spins. The increase of anisotropy field and the large field distribution due to the surface ferromagnetic layer lead to the large linewidth observed in the spectra. At high T, the FMR line shape is governed by the core anisotropy and the thermal fluctuations. On decreasing the temperature, the shell spins increase their magnetic moment, producing an effective field on the core leading to a decrease in the resonance field from its high T value. As the shell spins begin to order the effective anisotropy increases following the surface value more closely. This might directly affect the EMR linewidth increasing it to a higher than expected value. In contrast, no EPR signals are observed below 170 K, as shown in figure 10(b), in NCMO BULK as the sample enters into the anti-ferromagnetic phase while cooling from room temperature, and hence not detectable by X-band EPR [22]. Similar size induced EMR signals were also observed from PCMO 10, PCMO 20, PCMO 40(not shown).

The temperature dependence of the EMR spectral parameters were plotted for various compounds using the fitting parameters obtained from the above equation. Here our main aim is to show the results related to the thermal evolution of the EMR linewidths of various particle sizes. The temperature dependence of the EMR linewidth is plotted for NCMO 10, NCMO 20, NCMO 40 and NCMO BULK and is shown in figure 11(a). It is seen in this figure that the charge ordered phase, as indicated by the increase of the linewidth below T_{CO}, decreases with a decrease of particle size. It should be noted that although the static DC magnetization measurements (M–T) show a complete suppression of the charge ordered phase in NCMO 10 measured at 1T, as shown in the inset of figure 11(a), and in NCMO 20 [9], the temperature dependence of the EMR linewidth shows that *charge ordered fluctuations* are still present in NCMO 10 (weakly) and NCMO 20 (strongly). If there was no charge ordered phase present in NCMO 10 and NCMO 20, there would be no *shallow minimum/dip* in the temperature dependence of EMR linewidth, and the linewidth would be independent of temperature. Also worth noting from this figure is that the temperature (T_{CO}) at which the linewidth shows minimum shifts towards low temperatures with decreasing particle size, as indicated by an arrow, implies a decrease in the strength of the CO phase. Similar results were observed and plotted in the case of PCMO nanoparticles of various sizes and their comparison with the corresponding PCMO BULK was made, as shown in the figure 12(a). The decrease in T_{CO} with a decrease in particle size was observed and reported earlier from static DC magnetization measurements, and at the critical diameter (17 nm) the CO phase was shown to disappear completely [16]. Here, we argue that the presence/absence of the CO phase in nanoscale CO manganites purely depends upon the *timescale* of the probing technique. In another words, the CO phase is dynamic in nanoscale manganites, and could not be observed by other direct static measurements.

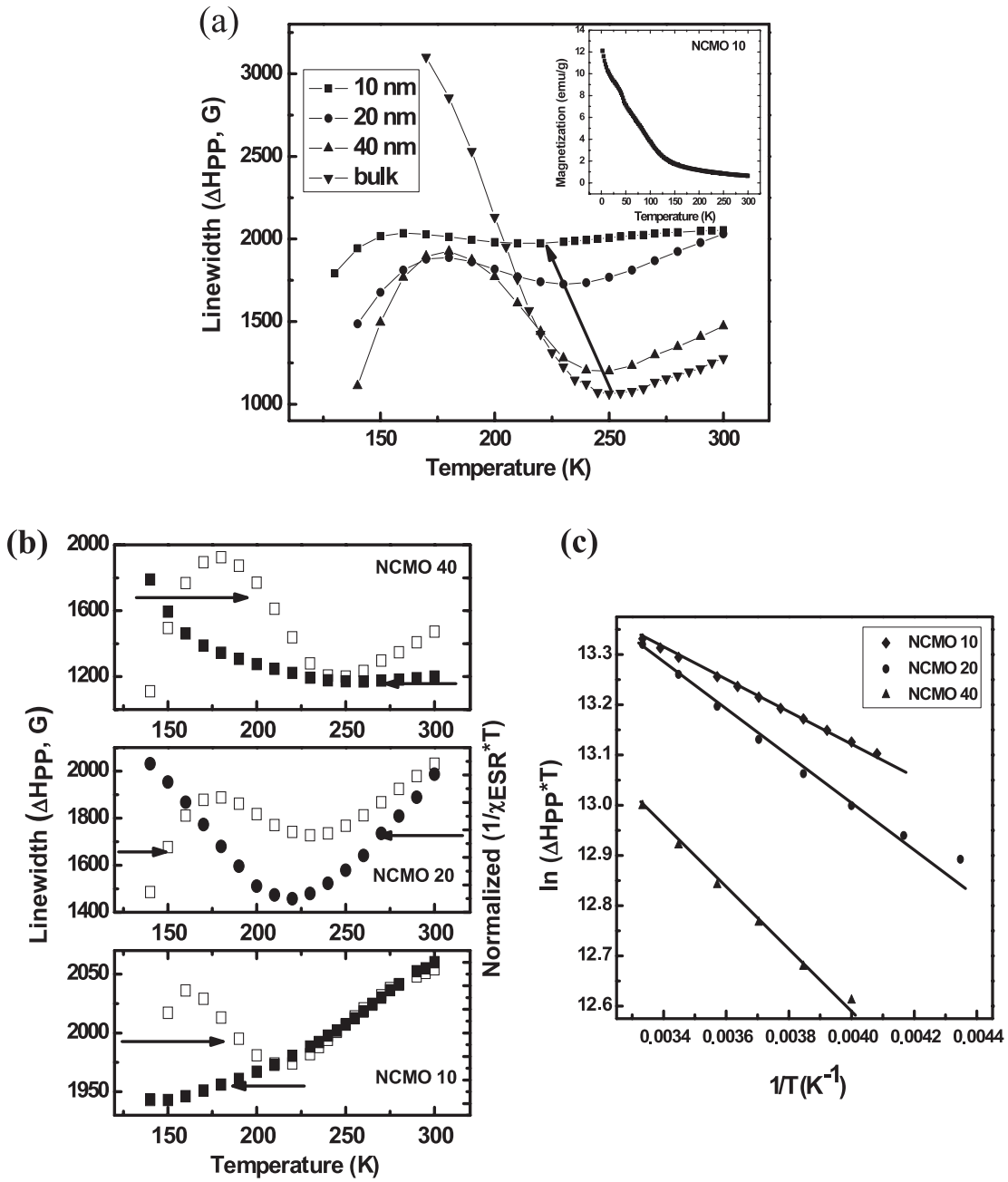

Figure 11. Temperature dependence of the EMR linewidth for NCMO 10, NCMO 20, NCMO 40 and NCMO BULK (a), the inset shows the variation of DC magnetization with temperature for NCMO 10, exhibiting the complete suppression of the CO peak at 250 K. Concerning the applicability of the Causa model [45] to the temperature dependent linewidth behaviour in the paramagnetic phase of the nanosamples, it is seen that the linewidth behaviour qualitatively follows the Causa model in the case of NCMO 10 and deviates from it for NCMO 20 and NCMO 40 (b). Fit (solid line) of temperature dependent linewidth (symbols) behaviour to Shengelaya's model [46] for NCMO 10, NCMO 20 and NCMO 40 (c).

From the above three distinct experimental results, the following facts are listed to give the evidence for the presence of a residual charge ordered anti-ferromagnetic phase mixed with the predominant size induced ferromagnetic phase.

(a) The presence of a 'shallow minimum' from the temperature dependence of EMR linewidth on the lowest particle size (NCMO 10/PCMO 10) measured indicating the residual presence of CO phase or charge ordered fluctuations, as was also reported in our earlier publication [18] on PCBMO nanoparticles.

(b) The presence of a residual charge ordered phase in NCMO 10 is supported by the three following observations resulting from the specially designed magnetization measurements. Firstly, the failure to obtain the classical saturation magnetization Ms (3.5 μ_β/f.u.) indicates that a residual charge ordered anti-ferromagnetic phase exists even in 10 nm particles. The classical saturation magnetization Ms (3.5 μ_β/f.u.) could not be obtained from NCMO 10, as the residual charge ordered phase present in this compound inhibits the complete conversion

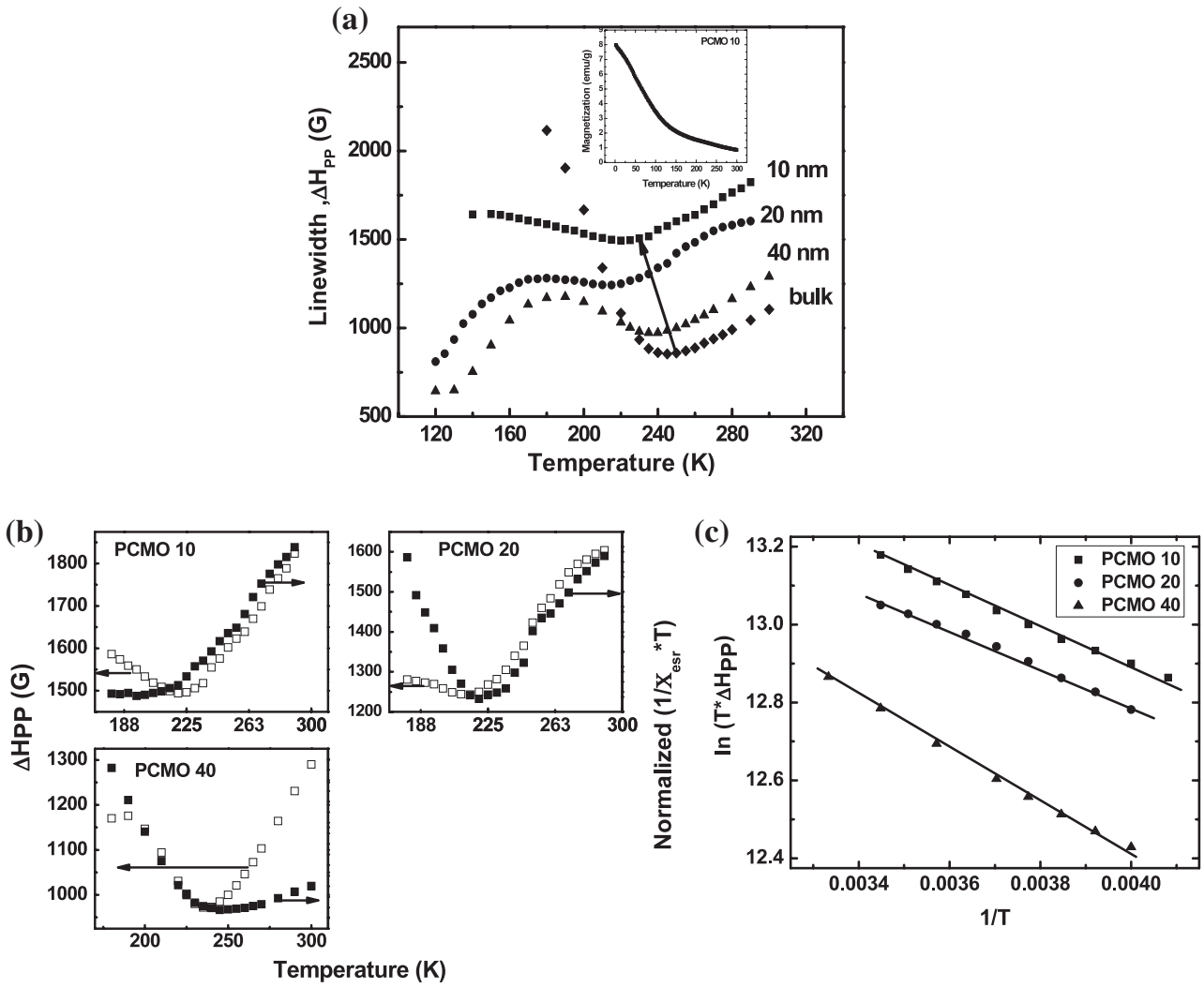

Figure 12. Temperature dependence of the EMR linewidth for PCMO 10, PCMO 20, PCMO 40 and PCMO BULK (a), the inset shows the variation of DC magnetization with temperature for PCMO 10, exhibiting the complete suppression of the CO peak at 245 K. Concerning the applicability of the Causa model [45] to the temperature dependent linewidth behaviour in the paramagnetic phase of the nanosamples, it is seen that the linewidth behaviour qualitatively follows the Causa model in the case of PCMO 10 and PCMO 20 and deviates from it for PCMO 40 (b). Fit (solid line) of temperature dependent linewidth (symbols) behaviour to Shengelaya's model [46] for PCMO10, PCMO20 and PCMO 40 (c).

of the AFM phase to the FM phase [29]. Secondly, the observed 'exchange bias' or 'M–H loop shift' (from figure 5) may arise because of the simultaneous presence of a residual charge ordered anti-ferromagnetic phase with the predominant size induced ferromagnetic phase [42]. Thirdly, the presence of anomalous M–H curves observed from NCMO 10 provides further direct evidence for a mixture of different magnetic phases; the FM phase being the predominant magnetic ground state [35].

(c) Another indication stems from the observation of both positive and negative magneto resistances resulting from the temperature dependent magneto-transport measurements (from figures 8(a) to 9(d)). This indicates that there is a simultaneous mixture of a ferromagnetic metallic phase with an anti-ferromagnetic charge ordered insulating phase, as reported [43] to originate from the ferromagnetic metallic and charge ordered anti-ferromagnetic insulating phases.

Very recently, the presence of a charge ordered phase has been detected and reported [44] in nanocrystalline $Pr_{0.65}(Ca_{0.7}Sr_{0.3})_{0.35}MnO_3$ through magneto calorimetric measurements, despite temperature dependent magnetic susceptibility and resistivity results have shown the absence of a charge ordered peak.

Here we discuss the nature of spin dynamics in nanoscale CO manganites with its temperature dependence by examining the applicability of two well known models available in the literature. For NCMO 10 the temperature dependence of linewidth in the paramagnetic phase follows the Causa model [45] and the test results are shown in figure 11(b). This model states that the linear temperature dependence of the linewidth in the paramagnetic phase is attributed to the spin–spin relaxation mechanism alone. According to this model,

$$\Delta H_{pp}(T) \propto 1/(\chi_{esr} T), \tag{2}$$

where χ_{esr} is the ESR intensity. For NCMO 10, the linewidth shows a minimum at $T_{CO} \sim 215$ K and increases with a further decrease in temperature, as is also observed in the CO phase of bulk manganites [21]. For NCMO 20 and NCMO 40, the temperature dependence of linewidth does not follow the Causa model, as shown in figure 11(b). This deviation might be the consequence of a more robust charge ordered phase in NCMO 20 and NCMO 40 in comparison with NCMO 10. We examined the applicability of Shengelaya's model or the bottleneck model (spin–lattice relaxation model) [46]

$$\Delta H_{pp}(T) = \Delta H_0 + (A/T)\exp(-Ea/K_B T), \qquad (3)$$

where the symbols have their usual meanings to the temperature dependent linewidth behaviour for NCMO 10, NCMO 20, NCMO 40. The test results are shown in figure 11(c). From this graph, it is seen that the later model describes the spin dynamics satisfactorily in nanoscale CO manganites. A similar analysis was carried out for PCMO 10, PCMO 20 and PCMO 40, and the results are depicted in figures 12(b) and (c). The activation energy obtained from this model is found to be 0.095 eV, and is close to the value (0.1 eV) obtained from the transport measurements. These results are consistent with our earlier published data [28], where it was shown that the spin dynamics in nanoscale manganites follow the bottleneck relaxation model. The exact mechanism for the linewidth behaviour is yet to be understood, as the spin relaxation mechanisms could be different on the surface and in the core of the nanosystems.

Here we discuss the size induced ESR line broadening and our attempts to measure the relaxation times for the above nanoscale charge ordered manganites. In the literature [22, 23, 39, 41], it was argued that an anti-symmetric exchange interaction, like the Dzyaloshinsky–Moria (DM) interaction, contributes predominantly to the EPR signal broadening in anti-ferromagnetic CO manganites observed in the charge disordered paramagnetic phase. Here, in this report, we show that EPR signal broadens further with a decrease in particle size by a factor of about 1.6 times from NCMO Bulk to NCMO 10 as measured at room temperature. In the literature, it had been shown that conventional pulse EPR spectrometers fail to detect the spin lattice relaxation times of manganites, hence highly innovative longitudinal modulation techniques [47–49] were used. The latter technique is employed here to unravel the origin of the enormous EMR signal broadening observed in nanoscale NCMO and PCMO manganites. In order to resolve this, with the help of Professor Atsarkin, we made an attempt to measure the electron spin lattice relaxation times ($T_1 = T_2$, for a exchange narrowed Lorentzian shaped EPR signal in a PM phase well above T_{CO}) on NCMO 20 by using the longitudinal modulation technique, which had been successfully applied to measure the T_1 of CMR manganites and various other materials, [47–49]. The sample under investigation was placed into a specially designed microwave cavity with its walls transparent to an rf (radio frequency) magnetic field in the MHz range. The microwave power, at the frequency of 9.3 GHz, was subjected to deep amplitude modulation, at a modulation frequency of 10^6 Hz, before entering the cavity. For further details about this technique it is suggested to refer to the extensive work done by Atsarkin *et al* [47–49]. The relaxation rate T_1^{-1}, proportional to the spectral density of the internal field fluctuations at the ESR frequency, can give information about magnetic correlations and other dynamical processes of interest which strongly influence the linewidth. We succeeded in measuring T_1 at two different low temperatures on NCMO 20 by adopting the procedure outlined elsewhere [47–49], although with much less accuracy (20–30%). The values obtained are $T_1 = 0.4$ ns at $T = 109$ K and $T_1 = 0.5$ ns at 80 K (below $T_c = 120$ K), corresponding to homogeneous line broadening, reached the limit of the technique as short as 10^{-9} to 10^{-10} s. Under the condition of strong exchange narrowing, the homogeneous half width reads as $\Delta_{hom} = 1/T_1 = 1/T_2 = 2.5 \times 10^9$ s^{-1} $= 4 \times 10^8$ Hz and the corresponding width is estimated as about 140 G. The observed EPR/EMR linewidth is much broader (1500–2000 G), as shown in the figure 11(a). This could be caused by a strong magnetic anisotropy due to surface and shape effects. The anisotropic axes of the particles are directed randomly, leading to strong inhomogeneous broadening, typical for randomly oriented magnetic nanoparticles. However, we could not succeed in measuring T_1 in the paramagnetic phase using this technique, as the EMR signals originating from NCMO 20 are too broad, and in addition there is a great decrease in the longitudinal magnetization response which further limits the sensitivity and scope of this technique.

No quantitative theory has yet been developed which could explain the origin of EPR linewidth, either in bulk or in nanoscale charge ordered manganites, except for a 'motional narrowing picture' in the charge ordered phase between T_N and T_{CO} [22]. In the absence of any reported observations made on EPR line broadening in nanoscale charge ordered manganites, here we present various possibilities which might lead to the EPR line broadening. One potential possibility could originate from consequences of large internal fields, Jahn–Teller (JT) effects and increase in DM interactions at the nanoscale as a result of high surface to volume ratio [50]. The enormous increase in linewidth with decreasing particle size might also be due to disorder present on the particle surface as a result of the competition between the various magnetic phases (magnetic frustration) at different length scales. Another possibility that deserves a mention here is the following. In the ensemble of magnetic nanoparticles the linewidth could be broadened by anisotropic spin interactions [51], as the anisotropy axis is randomly oriented. In addition the presence of surface and shape anisotropies would broaden the EPR linewidth further. At this time, it is difficult to resolve the individual contributions which add to the total linewidth. The identification of an appropriate line broadening mechanism is crucial to explore. This particular investigation demands a clear theoretical understanding of different interaction mechanisms such as DM interactions, the JT mechanism and the crystal field interaction, and sensitive experimental results in order to investigate the origin of EMR linewidth in nanoscale CO manganites. Unfortunately, our present knowledge is insufficient to explore the origin of EMR line broadening conclusively in these systems.

4. Conclusions

We have shown that the predominant ground state magnetic phase is ferromagnetic, coexisting with a residual antiferromagnetic phase, in nanoscale charge ordered manganites. The experimental observation of an exchange bias resulting from the magnetization measurements, the simultaneous occurrence of both positive and negative magneto resistance as observed from the field swept magneto-transport measurements, and the presence of a shallow minimum in the temperature dependence of the EMR linewidth give ample evidence for the presence of charge ordered fluctuations in nanoscale charge ordering manganites, in spite of the fact that the CO phase was shown to be absent/suppressed from the static DC magnetization (M–T) and transport (R–T) measurements. We have shown that the EMR line broadens significantly with a reduction in the particle size down to the nanoscale, and we have demonstrated that the 'bottleneck' relaxation model describes the spin dynamics satisfactorily in nanoscale charge ordered manganites. These interesting observations have to be explored further using other experimental techniques and theoretical methods. It is necessary to conduct low temperature transmission electron microscopy experiments to get the visual picture of the existence of residual charge order phase present in these nanoscale CO manganites.

Acknowledgments

SSR would like to acknowledge CSIR, Government of India for SRF. The authors are greatly indebted to Professor V A Atsarkin, IREE, Russia for his attempts to measure T_1 using the longitudinal modulation technique and for many useful discussions. The authors acknowledge Dr Ajay Sharma, MPI, Mainz, Germany for his attempts to measure T_1 using ESR X- and W-band pulse experiments, albeit unsuccessfully. DST, Government of India is acknowledged for funding the 14 T PPMS-VSM installed in IUC Indore and for the 12 T Janis made low temperature magneto-transport set up located at the Indian Institute of Science, Bangalore, India. SVB thanks DST, India for project funding under NSTI.

References

[1] Rao C N R and Raveau B (ed) 1998 *Colossal Magnetoresistance, Charge Ordering and Related Properties* (Singapore: World Scientific)
For a review see Tomioka Y and Tokura Y 2000 *Colossal Magnetoresistive Oxides* ed Y Tokura (New York: Gordon and Breach)
[2] Coey J M D, Viret M and von Molnaíar S 1999 *Adv. Phys.* **48** 167
[3] Ramakrishnan T V 2007 *J. Phys.: Condens. Matter* **19** 125211
[4] Lopez-Quintela M A, Hueso L E, Rivas J and Rivadulla F 2003 *Nanotechnology* **14** 212
[5] Zhang D, Liu Z, Han S, Li C, Lei B, Stewart M P, Tour J M and Zhou C 2004 *Nano Lett.* **4** 2151
[6] Levy P, Leyva A G, Troiani H E and Sánchez R D 2003 *Appl. Phys. Lett.* **83** 5247
[7] Curiale J, Sánchez R D, Troiani H E, Leyva A G and Levy P 2005 *Appl. Phys. Lett.* **87** 043113
[8] Rao S S, Anuradha K N, Sarangi S and Bhat S V 2005 *Appl. Phys. Lett.* **87** 182503
[9] Rao S S, Tripathi S, Pandey D and Bhat S V 2006 *Phys. Rev.* B **74** 144416
[10] Kuwahara H, Tomoika Y, Asamitsu A, Moritomo Y and Tokura Y 1995 *Science* **270** 961
[11] Moritomo Y, Kuwahara H, Tomoika Y and Tokura Y 1997 *Phys. Rev.* B **55** 7549
[12] Dong S, Gao F, Wang Z Q, Liu J M and Ren Z F 2007 *Appl. Phys. Lett.* **98** 082508
[13] Lu C L, Dong S, Wang K F, Gao F, Li P L, Lv L Y and Liu J M 2007 *Appl. Phys. Lett.* **91** 032502
[14] Gao F, Li P L, Weng Y Y, Dong S, Wang L F, Lv L Y, Wang K F and Liu J M 2007 *Appl. Phys. Lett.* **91** 072504
[15] Sarkar T, Raychaudhuri A K and Chatterji T 2008 *Appl. Phys. Lett.* **92** 123104
[16] Zhang T, Zhou T F, Qian T and Li X G 2007 *Phys. Rev.* B **76** 174415
[17] Dong S, Yu R, Yunoki S, Liu J M and Dagotto E 2008 *Phys. Rev.* B **78** 064414
[18] Anuradha K N, Rao S S, Sharma A and Bhat S V 2008 *Appl. Magn. Reson.* **33** 127
[19] Oseroff S B, Torikachvili M, Singley J, Ali S, Cheong S W and Schultz S 1996 *Phys. Rev.* B **53** 6521
[20] Huber D L, Alejandro G, Caneiro A, Causa M T, Prado F, Tovar M and Oseroff S B 1999 *Phys. Rev.* B **60** 12155
[21] Shames A I, Rozenberg E, McCarroll W H, Greenblatt M and Gorodetsky G 2001 *Phys. Rev.* B **64** 172401
[22] Joshi J P, Gupta R, Sood A K, Bhat S V, Raju A R and Rao C N R 2001 *Phys. Rev.* B **65** 24410
[23] Joshi J P, Sarathy K V, Sood A K, Bhat S V and Rao C N R 2000 *J. Phys.: Condens. Matter* **16** 2869
[24] Rao S S and Bhat S V 2009 *J. Phys. D: Appl. Phys.* **42** 075004
[25] Anuradha K N, Rao S S and Bhat S V 2007 *J. Nanosci. Nanotechnol.* **7** 1775
[26] Tokunaga M, Miura N, Tomioka Y and Tokura Y 1998 *Phys. Rev.* B **57** R9377
[27] Millange F, de Brion S and Chouteau S 2000 *Phys. Rev.* B **62** 5619
[28] Rao S S, Padmanabhan B, Elizabeth S, Bhat H L and Bhat S V 2008 *J. Phys. D: Appl. Phys.* **41** 155011
[29] Curiale J, Sanchez R D, Troiani H E, Ramos C, Pastoriza H, Leyva A G and Levy P 2007 *Phys. Rev.* B **75** 224410
[30] Dong S, Gao F, Wang Z Q and Liu J M 2007 *Appl. Phys. Lett.* **90** 082508
[31] Zysler R D, Ramos C A, De Biasi E, Romero H, Ortega A and Fiorani D 2000 *J. Magn. Magn. Mater.* **221** 37
[32] Tronc E, Ezzi A, Cherkaoui R, Chaneac C, Nogues M, Kachkachi H, Fiorani D, Testa A M, Greneche J M and Jolivet J P 2000 *J. Magn. Magn. Mater.* **221** 63
[33] Manekar M A, Chaudhary S, Chattopadhyay M K, Singh K J, Roy S B and Chaddah P 2001 *Phys. Rev.* B **64** 104416
[34] Zhang Y Q, Zhang Z D and Aarts J 2005 *Phys. Rev.* B **70** 132407
[35] Banerjee A, Mukherjee K, Kumar K and Chaddah P 2006 *Phys. Rev.* B **74** 224445
[36] Banerjee A, Pramanik A K, Kumar K and Chaddah P 2006 *J. Phys.: Condens. Matter* **18** L605
[37] Venkataiah G, Krishna D C, Vitha M, Rao S S, Bhat S V, Prasad V, Subramanyam S V and Venugopal Reddy P 2005 *Physica* B **357** 370
[38] Zhu M H, Zhao Y G, Cai W, Wu X S, Gao S N, Wang K, Luo L B, Huang H S and Lu L 2007 *Phys. Rev.* B **75** 134424
[39] Joshi J P, Sood A K, Bhat S V, Parashar S, Raju A R and Rao C N R 2004 *J. Magn. Magn. Mater.* **279** 91
[40] Joshi J P and Bhat S V 2004 *J. Magn. Reson.* **168** 284
[41] Sharma A, Sarangi S and Bhat S V 2006 *Phys. Rev.* B **73** 035129
[42] Huang X H, Ding J F, Zhang G Q, Hou Y, Yao Y P and Li X G 2008 *Phys. Rev.* B **78** 224408 and references there in
[43] Mahendiran R, Mahesh R, Gundakaram R, Raychaudhuri A K and Rao C N R 1996 *J. Phys.: Condens. Matter* **8** L455
[44] Biswas A, Samanta T, Banerjee S and Das I 2008 *Appl. Phys. Lett.* **92** 212502

[45] Causa M T, Tovar M, Caneiro A, Prado F, Ibanez G, Ramos C A, Butera A, Alascio B, Obradors X, Pinol S, Rivadulla F, Vazquez-Vazquez C, Lopez-Quintela C A, Rivas J, Tokura Y and Oseroff S B 1998 *Phys. Rev.* B **58** 3233

[46] Shengelaya A, Zhao G-M, Keller H, Muller K A and Kochlev B I 2000 *Phys. Rev.* B **61** 5888

[47] Atsarkin V A, Demidov V V, Simon F, Gaal R, Moritomo Y, Conder K, Janossy A and Forro L 2003 *J. Magn. Magn. Mater.* **258** 256–8

[48] Atsarkin V A, Demidov V V and Vasneva G A 1995 *Phy. Rev.* B **52** 1290

[49] Atsarkin V A, Demidov V V, Vasneva G A and Conder K 2001 *Phys. Rev.* B **63** 092405

[50] Köseoğlu Y, Yildiz F, Salazar-Álvarez G, Toprak M, Muhammed M and Akta B 2005 *Phys. Status Solidi* b **242** 1712

[51] Dutta P, Seehra M S, Thota S and Kumar J 2008 *J. Phys.: Condens. Matter* **20** 015218